Mobius3D

The complete patient QA system

3D patient plan QA

3D IMRT/VMAT pre-treatment QA

3D in vivo daily treatment QA

Online patient positioning QA

Upgrade your patient safety by bridging the gap between patient QA and machine QA

DoseLab® machine QA software, the complete TG-142 solution, is now integrated into the Mobius3D® patient QA system!

Visit mobiusmed.com/mobius3d to learn more.

Safety information: Radiation may cause side effects and may not be appropriate for all cancers.

varian | MOBIUS

Internal breast dosimetry in mammography: Experimental methods and Monte Carlo validation with a monoenergetic x-ray beam

Christian Fedon
Department of Radiology and Nuclear Medicine, Radboud University Medical Center, PO Box 9101 6500 HB Nijmegen, The Netherlands
Istituto Nazionale di Fisica Nucleare (INFN) sezione di Trieste, 34127 Trieste, Italy

Marco Caballo
Department of Radiology and Nuclear Medicine, Radboud University Medical Center, PO Box 9101 6500 HB Nijmegen, The Netherlands

Renata Longo
Istituto Nazionale di Fisica Nucleare (INFN) sezione di Trieste, 34127 Trieste, Italy
Dipartimento di Fisica, Università degli Studi di Trieste, 34127 Trieste, Italy

Annalisa Trianni
Medical Physics Department, Azienda Sanitaria Universitaria Integrata (ASUIUD) – Presidio Ospedaliero "S. Maria della Misericordia", p.le S. Maria della Misericordia, 15 33100 Udine, Italy

Ioannis Sechopoulos[a)]
Department of Radiology and Nuclear Medicine, Radboud University Medical Center, PO Box 9101 6500 HB Nijmegen, The Netherlands
Dutch Expert Center for Screening (LRCB), PO Box 6873 6503 GJ Nijmegen, The Netherlands

(Received 25 July 2017; revised 5 December 2017; accepted for publication 19 January 2018; published 23 February 2018)

Purpose: To investigate the performance, such as energy dependence and sensitivity, of thermoluminescent dosimeters (TLD), metal oxide semiconductor field-effect transistor dosimeters (MOSFET), and GafChromic™ films, and to validate the estimates of local dose deposition of a Monte Carlo (MC) simulation for breast dosimetry applications.
Methods: Experimental measurements were performed using a monoenergetic beam at the ELETTRA synchrotron radiation light source (Trieste, Italy). The three types of dosimeters were irradiated in a plane transversal to the beam axis and calibrated in terms of air kerma. The sensitivity of MOSFET dosimeters and GafChromic™ films was evaluated in the range of 18–28 keV. Three different calibration curves for the GafChromic™ films were tested (logarithmic, rational, and exponential functions) to evaluate the best-fit curve in the dose range of 1–20 mGy. Internal phantom dose measurements were performed at 20 keV for four different depths (range 0–3 cm, with 1 cm steps) using a homogeneous 50% glandular breast phantom. A GEANT4 MC simulation was modified to match the experimental setup. Thirty sensitive volumes, on the axial-phantom plane were included at each depth in the simulation to characterize the internal dose variation and compare it to the experimental TLD and MOSFET measurements. Experimental 2D dose maps were obtained with the GafChromic™ films and compared to the simulated 2D dose distributions estimated with the MC simulations.
Results: The sensitivity of the MOSFET dosimeters and GafChromic™ films increased with x-ray energy, by up to 37% and 48%, respectively. Dose–response curves for the GafChromic™ film result in an uncertainty lower than 5% above 6 mGy, when a logarithmic relationship is used in the dose range of 1–10 mGy. All experimental values fall within the experimental uncertainty and a good agreement (within 5%) is found against the MC simulation. The dose decreased with increasing phantom depth, with the reduction being ~80% after 3 cm. The uncertainty of the empirical measurements makes the experimental values compatible with a flat behavior across the phantom slab for all the investigated depths, while the MC points to a dose profile with a maximum toward the center of the phantom.
Conclusions: The calibration procedures and the experimental methodologies proposed lead to good accuracy for internal breast dose estimation. In addition, these procedures can be successfully applied to validate MC codes for breast dosimetry at the local dose level. The agreement among the experimental and MC results not only shows the correctness of the empirical procedures used but also of the simulation parameters. © *2018 The Authors Medical Physics published by Wiley Periodicals, Inc. on behalf of American Association of Physicists in Medicine.* [https://doi.org/10.1002/mp.12792]

Key words: breast dosimetry, GafChromic™ film, GEANT4, MOSFET, TLD

1. INTRODUCTION

Mammography is currently the reference technology for early detection of breast cancer. Millions of women undergo mammography examinations every year for both early detection (i.e., screening) and diagnosis. Due to the use of mammography as a screening technique, characterization and optimization of the radiation dose delivered is extremely important.

The current dose metric used in mammography is the mean glandular dose (MGD).[1] However, a direct measurement of MGD is not feasible. The MGD is estimated using conversion factors[2,3] obtained with Monte Carlo (MC) simulations which relate air kerma to the average dose absorbed by the glandular tissue. Recent studies have shown that current breast dosimetry models tend to overestimate patient breast dose due to the uniform homogeneous approximation of the internal adipose/glandular breast tissue mixture.[4–6] Therefore, it is expected that a new breast model for dosimetry could involve a nonuniform and/or nonhomogeneous tissue description. A new breast model for dosimetry is one of the aims of the Task Group No. 282 recently formed by the American Association of Physicists in Medicine (AAPM) and the European Federation Of Organization for Medical Physics (EFOMP).[7] This work has been performed within this context.

Consequently, this work has two aims: (a) to develop accurate methods to experimentally estimate the internal breast radiation dose distribution and (b) to accurately validate MC estimates of local dose deposition throughout the breast experimentally. This task is complicated due to the nuances in experimental conditions (such as variation in the sensitivity and the energy dependence of the dosimeter, heel effects, scatter correction factors, etc.) and the corresponding uncertainties.[8] MC code for breast dosimetry has often been validated considering average (or ratio) quantities[5,9,10] or comparing the MC output against a software-based reference, such as the report of the Task Group 195.[8] However, one of the aims of this study is the experimental validation of MC code for breast dosimetry at the level of local dose deposition and in absolute terms.

To perform this validation, dosimeters based on three different technologies were used to measure the radiation dose in mammography: thermoluminescent dosimeters (TLDs),[11,12] metal oxide semiconductor field-effect transistor (MOSFET),[13,14] and GafChromic™ films.[15] Multiple dose measurements and tests (e.g., for TLDs and MOSFET sensitivity tests while for GafChromic™ films, scanner homogeneity, best-film size for the calibration, calibration curves analysis, reproducibility, etc.) were used so as to optimize the methodology of their use and also characterize the performance of each for this low-dose and low-energy application.

Several authors characterized these dosimeters in terms of energy and dose–response.[16–21] However, a comprehensive review of the procedures to follow with these technologies for internal breast dosimetry estimation and of their capabilities in this application, is, to the best of our knowledge, not currently available.

Monoenergetic photons from synchrotron radiation (SR) offer a suitable benchmark for testing dosimeters and MC performance without the compounding effects of conventional x-ray sources (e.g., spectral distribution, beam hardening, heel effect, etc.). Moreover, improving our knowledge of these dosimeters with SR could be beneficial due to the increasing use of SR for medical applications.[22–27]

Therefore, in this work, three different dosimeters (TLD-100H, MOSFET type TN-1002RD, and XR-QA2 GafChromic™ films) are tested in the monoenergetic range interval of 18–28 keV. Calibration procedures and energy dependence are presented. A homogeneous semi-cylindrical phantom, which mimics a 50% glandular breast, is used to investigate the internal dose distribution at the monochromatic energy of 20 keV and to validate MC-based estimations of local breast dose deposition.

The uncertainty of the experimental values is treated according to the IAEA report TRS 457,[28] which is based on the Guide on the Expression of Uncertainty in Measurement (GUM).[29] Therefore, all the uncertainties are presented in a 68% confidence interval (i.e., coverage factor "k" = 1).

2. MATERIALS AND METHODS

2.A. Experimental setup at the SYRMEP beamline

Measurements were performed at the SYRMEP (SYnchrotron Radiation for MEdical Physics) beamline[30] of the ELETTRA synchrotron light source in Trieste, Italy (Fig. 1).

The polychromatic radiation source is one of the ELETTRA storage ring bending magnets. Monochromatic radiation is obtained by means of a Si(111) double-crystal monochromator working in Bragg configuration. The useful energy range is 8.5–40 keV, with an energy resolution ($\Delta E/E$) in the order of 10^{-3} for this energy interval. The beam divergence is about 7 mrad (horizontal) × 40 μrad (vertical) and the radiation source to phantom position distance is about 30 m (of which 26.5 m in vacuum). Thus, the SR beam can be considered a parallel beam. A system of tungsten slits (i.e., vacuum/air slits in Fig. 1) is used to define the beam shape, which reaches a maximum cross-section of 22 cm (horizontal) × 0.3 cm [vertical, Gaussian shape, full-width-at-half-maximum (FWHM)] at the phantom position.

Two custom-made, parallel-plate ionization chambers (IOC1 and IOC2 in Fig. 1) provide a measurement of the air kerma at the phantom position. These two chambers were calibrated against the air kerma primary standard for low-energy x rays by the Department of Ionizing Radiation Metrology of the National Agency for New Technologies, Energy and Environment (ENEA-INMRI, Casaccia, Roma, Italy) in the energy range 8–28 keV.[31] This calibration range is going to be extended up to 40 keV to allow for the application of the SR to the breast computed tomography.[27]

Due to the vertical height of the laminar beam at the phantom position (typically 0.3 cm), the sample has to be vertically translated to accomplish a full irradiation. This is obtained by positioning the phantom between the plates of a compression system, and then moved the all system vertically with a constant speed.

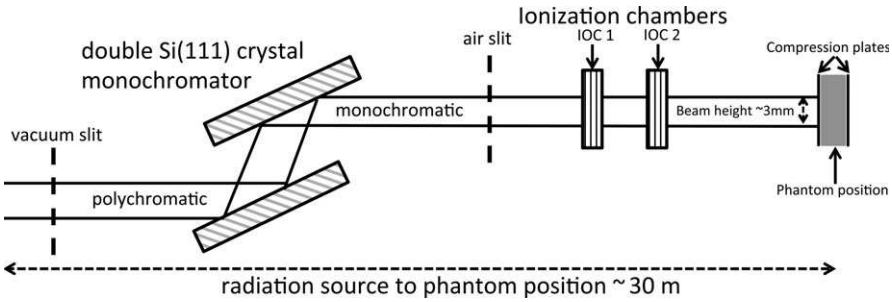

FIG. 1. Schematic side view of the SYRMEP beamline. The polychromatic beam is monochromatized by means of a double-crystal monochromator. The beam shape is defined by a system of tungsten slits, reaching a height of about 3 mm at the phantom position. Two ionization chambers (IOC 1 and IOC 2) provide a measurement of the air kerma. The diagram is not drawn to scale.

All measurements were performed using a homogeneous semi-cylindrical phantom (CIRS Inc., Norfolk, VA, USA) consisting of a collection of 1-cm-thick slabs, which reproduced the 50% glandular breast material (Fig. 2).

The placement of the dosimeters on the breast phantom is shown in Fig. 2(a): fixed positions were selected on the *xy* phantom plane in order to evaluate the dose distribution. Dose distributions were investigated at four different depths [Fig. 2(b)].

In the case of TLD and MOSFET dosimeters, for each depth, the dosimeters were placed in the fixed positions depicted in Fig. 2(a). The measurement was then repeated three times in order to average the final value. In the case of GafChromic™ films no averaging was performed. All the dosimeters were calibrated free-in-air in terms of air kerma against the absolute calibrated ionization chambers of the SYRMEP beamline.

2.B. GafChromic™ films: XR-QA2

XR-QA2 GafChromic™ (Ashland, USA) films are currently used as a quality assurance tool for radiology applications. The film consists of a 25-μm sensitive layer attached to a 20-μm acrylic adhesive. Both of those layers are sandwiched between a 97-μm orange-polyester layer (on top) and a 97-μm white polyester layer (on the bottom). The inclusion of a high Z element (i.e., Bismuth) in the sensitive layer increases the film sensitivity to lower x-ray energies, enhancing the photoelectric cross-section. Thus, the XR-QA2 films can be used to investigate the 2D-dose distribution in the low-energy range of mammography.

The GafChromic™ films require digitization in a reflective modality in order to evaluate the changes in optical reflectance. An Epson Perfection V750 flat bed scanner was used in reflectance mode to scan the films. All the automatic image adjustment features on the scanner control panel were disabled. The image resolution was set to 72 dpi (about 0.35 mm/pixel), since it was noted that there are no advantages when using higher resolution.[32] Images were saved as tagged image file format (TIFF) in a 48-bit RGB mode. Only the red component was extracted from the image file, since the sensitivity of XR-QA2 is higher in the red channel. The uniform response of the scanner was tested by scanning ten times a neutral sheet of pure white matte paper covering the entire scan bed. To better homogenize the pressure over the scanner, a PMMA slab ($21 \times 30 \times 2$ cm^3) was positioned on the paper during each scan. The advantage of using a white paper with a stable behavior over time has been discussed in the literature.[33–35] An average image was obtained and then divided into rectangular regions of interest (ROIs): 21 vertical ROIs (about 1×30 cm^2) and 29 horizontal ROIs (about 22×1 cm^2). ROI mean profiles were compared with the average value of the scanned area and scanned regions with a difference greater than 1% were avoided. A rectangular area (12×10 cm^2) with uniform response was identified at the scanner center and an opaque mask was positioned on the scanner glass in order to use only this homogeneous response area.[36]

Prior to any scanning session, five blank scans were made in order to warm up the scanner. The PMMA slab was

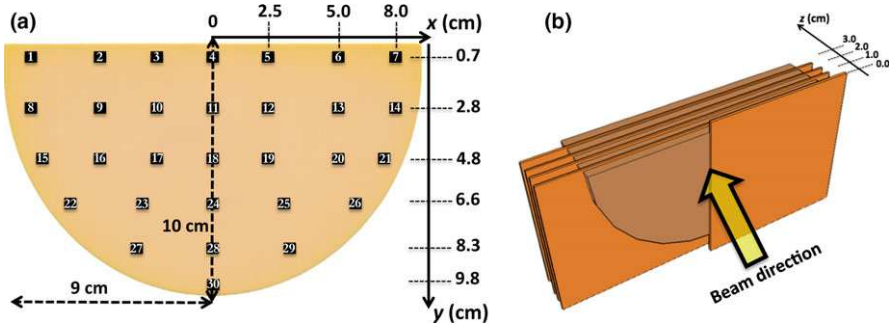

FIG. 2. (a) Dosimeter placement on the *xy* plane of the breast phantom. (b) Angled view of the four investigated depths (0, 1, 2, 3 cm) along the *z* direction. The compression system is not shown for clarity. [Color figure can be viewed at wileyonlinelibrary.com]

positioned on the GafChromic™ film during each scan. This procedure prevents some scanning artifacts, such as the so-called Newton rings. A single lot of XR-QA2 films was used throughout this work.

Analysis of the GafChromic™ film was performed using open source software (ImageJ, National Institutes of Health, Bethesda, MD, USA). The first step in the image analysis was the application of a median filter with a 3 × 3 pixel kernel: this procedure reduces the impulse noise in the image and removes any single dead pixels.[36] The film response was then evaluated in terms of reflectance change, according to the method proposed by Tomic et al.[20,37] The final film net reflectance change, netΔR, was defined as

$$net\Delta R = \Delta R - \Delta R^{Control} \tag{1}$$

where ΔR is the reflectance change for a film exposed to x rays, calculated as

$$\Delta R = \tilde{} \frac{1}{2^{16}} \left[PV_{Before} - PV_{After} \right] \tag{2}$$

and $\Delta R^{Control}$ is calculated using Eq. (2) for an unexposed control film, which quantifies reflectance changes due to effects other than those due to x-ray exposure. PV_{Before} and PV_{After} are the mean pixel values estimated before and after exposure, respectively, in a ROI of 1 × 1 cm^2. The corresponding uncertainty was defined as

$$\sigma_{net\Delta R} = \sqrt{(\sigma_{\Delta R})^2 + (\sigma_{\Delta R_{Control}})^2} \tag{3}$$

where $\sigma_{\Delta R}$ or $\sigma_{\Delta R_{Control}}$ are calculated as

$$\sigma_{\Delta R} = \frac{1}{2^{16}} \sqrt{\left(\sigma_{PV_{Before}}\right)^2 + \left(\sigma_{PV_{After}}\right)^2} \tag{4}$$

and $\sigma_{PV_{Before}}$, $\sigma_{PV_{After}}$ are the corresponding standard deviations estimated in the above-mentioned ROIs. All films were scanned 24 h after irradiation.

The XR-QA2 films were calibrated in terms of net reflectance change (netΔR) within the ROI versus the air kerma measured in air at the plane where the films were positioned. For the calibration procedure, three film pieces (3 cm × 3 cm), cut from a single sheet, were simultaneously irradiated free-in-air in a plane perpendicular to the beam at 20 keV. A uniform film exposure was obtained by moving the support at a constant speed across the beam. Ten different air kerma values were used to build the calibration curve in the dose range 1–20 mGy, and three different functions were investigated:

−logarithmic function: $y = a + \frac{bx}{\ln x}$
−rational function: $y = \frac{ax}{1+bx}$
−exponential function:

$$y = axe^{mx} \tag{5}$$

The precision of the above-mentioned calibration functions was tested following the procedure proposed by Devic et al.[38] According to this method, the overall dose uncertainty consists of two terms: the experimental uncertainties (e.g., measurement reproducibility, scan reproducibility, film nonuniformity, etc.), and the uncertainty due to the fitting process (e.g., uncertainty on the fit parameters). Once the best-calibration curve was identified, the associated uncertainty data points were fit to another function, using commercial software (TableCurve 2D, Systat Software Inc., Chicago, IL and SPSS Statistic 20.0, International Business Machines Corp., Armonk, NK).

The energy-dependent response of the films was assessed following the same procedure already presented for calibration, irradiating simultaneously free-in-air three film pieces (3 cm × 3 cm) cut from a single sheet. These measurements were performed in the energy interval from 18 to 28 keV (with an energy step of 1 keV), and at a nominal air kerma of ~3.5 mGy. The film sensitivity was defined as the ratio between the change in pixel values [i.e., netΔR in Eq. (1)] and the delivered air kerma.

In order to obtain a 2D dose map within the homogeneous phantom at different depths, a piece of film larger than the phantom was used (12 cm × 10 cm). The size was chosen so as to fit the uniform response scanner area, and to avoid any possible mechanical stress due to the cutting of the film. This necessitated the use of two pieces to cover the entire phantom: each piece was separately irradiated and the two resulting images were reassembled using an algorithm developed in MATLAB (The MathWorks, Natick, MA, USA). The previously described procedure was used to calculate the netΔR [see Eqs. (1) and (2)].

The 2D dose map (in mGy) was then obtained using the best-calibration fit function [i.e., logarithm function in Eq. (5)]. The combined standard uncertainty (k = 1) is expressed as follows:

$$u_{GAF} = \sqrt{u_{ROI}^2 + u_{Calib}^2 + u_{IOC}^2} \tag{6}$$

where u_{ROI}^2 is a Type A uncertainty for a 1-cm^2 ROI while u_{Calib}^2 and u_{IOC}^2 are Type B uncertainties for the calibration and IOC, respectively, estimated on a rectangular-based distribution.

Table I summarizes the procedures for the GafChromic™ films.

2.C. Metal oxide semiconductor field-effect transistor: MOSFET

Five high-sensitivity, metal oxide semiconductor field-effect transistor (MOSFET) dosimeters, model TN-1002RD (Best Medical Canada Ltd., Ottawa, Canada) were used in this work. A typical MOSFET dosimeter consists of a rectangular kapton support (0.25 cm × 0.76 cm) on which an epoxy bulb of 0.1-cm thickness contains the sensitive layer (i.e., SiO_2).[14,19] The dosimeters were used in conjunction with the Patient Dose Verification System (model No. TN-RD-16) with the high-sensitivity bias supply.

TABLE I. Summary of the GafChromic™ film (XR-QA2 model) experimental procedure.

Procedure	Actions
1. Scanner uniform area	• Warm up the scanner before each use (e.g., with five empty scans) • Identify the uniform response area of the scanner by scanning ten times a neutral sheet of pure white matte paper covering the entire scan bed[35] • If needed, place over the paper a weight to better homogenize the pressure, for example, with a 2-cm-thick piece of PMMA, of at least the size of the film • Obtain an average image from the 10 scans and then divide it into rectangular ROIs (e.g., 21 vertical ROIs of 1 × 30 cm^2 and 29 horizontal ROIs of 22 × 1 cm^2) • Compare the mean profile of the ROIs with the average value of the scanned area • Avoid all the regions with a difference greater than 1%
2. Calibration preparation	• Cut the GafChromic™ sheet in square pieces of 3 cm × 3 cm • Use three film pieces for each calibration point (e.g., 7 points in the dose range 1–10 mGy, requiring 21 pieces + 3 pieces for the background subtraction) • Consistently and preferably expose films with the orange layer facing the x-ray source • Warm up the scanner before each use (e.g., with five empty scans) • Scan each piece paying attention to use the homogeneous central area of the scanner • If needed, place over the film a weight to better homogenize the pressure, for example, with a 2-cm-thick piece of PMMA, of at least the size of the film. • Turn off the image adjustment features of the scanner and use 72 dpi scanning resolution, saving the image as TIFF file format in 48-bit RGB mode
3. Calibration analysis	• Apply a median filter with a 3 × 3 pixel kernel to each scan • Select a central ROI of 1 cm^2 (i.e., 28 × 28 $pixels^2$) to avoid the mechanical stress due to the cutting at the edges of the films (~1 cm) • Evaluate the film-reflectance change using the method proposed by Tomic et al.[20,37] (see Section 2.B.) • Fit the calibration points using a logarithmic function $\left(\text{i.e. } y = a + \frac{bx}{\ln x}\right)$ to obtain the calibration curve • Evaluate the calibration uncertainty using the procedure proposed by Devic et al.[38] (see Section 2.B.)
4. Phantom measurements	• Cut the GafChromic™ sheet to a size larger than your phantom to avoid the mechanical stress due to the cutting at the edges of the films (~1 cm). Pay attention that the GafChromic™ piece fits the uniform response scanner area (otherwise use multiple pieces) • Apply a median filter with a 3 × 3 pixel kernel to each scan • Evaluate the film-reflectance change using the method proposed by Tomic et al.[20,37] • Evaluate the combined standard uncertainty

The signal response (ΔV) of each MOSFET was determined by the difference between the pre- (V_{pre}) and postexposure (V_{post}) voltages. The *i*-th dose for a single MOSFET dosimeter was evaluated according to the following equation

$$D_i = \frac{\Delta V_i}{CF_i} \tag{7}$$

where CF_i is the calibration factor (in mV/mGy) for the *i*-th MOSFET, obtained as the difference in voltage to a known air kerma. A final dose value ($\overline{D_{MOSFET}}$) was obtained by averaging three exposures. To ensure consistency, the same MOSFET dosimeter was always exposed at the same positions [Fig. 2(a)].

The combined standard uncertainty (k = 1) for $\overline{D_{MOSFET}}$ is expressed as follows:

$$u_{\overline{D_{MOSFET}}} = \sqrt{u^2_{\Delta V} + u^2_{CF} + u^2_{IOC} + u^2_{MOSFET}}. \tag{8}$$

where $u^2_{\Delta V}$ and u^2_{CF} are Type A uncertainties for the signal response and calibration factor, respectively [see Eq. (7)]; and u^2_{IOC} and u^2_{MOSFET} are Type B uncertainties for the IOC and MOSFET accuracy, respectively, all estimated on a rectangular-based distribution.

The energy dependence was determined by irradiating the dosimeters free-in-air in a plane perpendicular to the beam at a range of energies, varying from 18 to 28 keV (with energy steps of 1 keV). A uniform exposure was obtained by moving the support at a constant speed. The sensitivity was calculated as the ratio between the voltage difference (i.e., ΔV) and the air kerma that caused this change (i.e., nominal value of 3.8 mGy).

Table II summarizes the procedures for the MOSFET.

2.D. Thermoluminescent dosimeters

High-sensitivity lithium fluoride (LiF: Mg, Cu, P) thermoluminescent dosimeters chips (TLD-100H, ThermoFisher Scientific, Waltham, MA, USA) were used in this study. According to manufacturer specifications, the detection range for these chips is 1 to 10 Gy. The chip dimensions are 3.2 mm × 3.2 mm, with a thickness of 0.38 mm. The annealing and reading procedures were performed using a TLD reader (Harshaw Model 3500, Thermo Electron Corporation, Solon, OH, USA) according to the manual. Specifically, the time–temperature profile involved preheating the sample to 135°C for 10 s; in the acquisition phase the sample was heated for 23 1/3 s to 240°C with a linear ramp rate of 10°C/s followed by an annealing phase of 10 s at 240°C. To improve the accuracy of low-exposure readings, nitrogen gas was applied during the whole cycle.

The dose evaluated for the *i*-th TLD is provided by the following equation:

TABLE II. Summary of the MOSFET (TN-1002RD model) experimental procedure.

Procedure	Actions
1. Calibration	• Place the MOSFET with the black-epoxy bulb facing the x-ray source • Evaluate the calibration factors separately for each device • Obtain the calibration factors as the difference in voltage to a known air kerma
2. Phantom measurements	• Place the MOSFET with the black-epoxy bulb facing the x-ray source in the design position within the phantom • Evaluate the dose value by averaging three exposures • Evaluate the combined standard uncertainty

$$D_i^{TLD} = Q_i \mathrm{x} \frac{K_{calib}}{S_i}. \quad (9)$$

where Q_i is the i-th TLD reading (in nC), S_i is a dimensionless-sensitivity factor and K_{calib} is the calibration factor (in mGy/nC). The S_i factor is specific for each TLD and it is meant to correct for the natural variations in TLD material response and for the variation in the physical mass of the chips. It is applied to make the response of each dosimeter comparable to the average response of all TLDs. The S_i factor was calculated by exposing all the TLDs free-in-air to the same radiation field and taking the ratio between the i-th reading and the average-sample reading. K_{calib} was obtained by exposing three TLDs free-in-air at four different air kerma values. No correction was made for the TLD self-absorption since, at this energy, the TLD thickness was assumed not to attenuate the beam to a significant degree.[39]

At each phantom position [Fig. 2(a)], a final mean dose value ($\overline{D_{TLD}}$) was calculated by averaging over three TLD values [i.e., D_i^{TLD} in Eq. (9)].

The combined standard uncertainty (k = 1) is expressed as follows:

$$u_{\overline{D_{TLD}}} = \sqrt{u_Q^2 + u_S^2 + u_{K_{calib}}^2 + u_{IOC}^2 + u_{TLD-reader}^2} \quad (10)$$

where u_Q^2, u_S^2 and $u_{K_{calib}}^2$ are Type A uncertainties for the reading, sensitive factor and calibration factor, respectively, while u_{IOC}^2 and $u_{TLD-reader}^2$ are Type B uncertainties for the IOC and TLD reader accuracy, respectively, again estimated on a rectangular-based distribution.

Table III summarizes the procedures for the TLDs.

TABLE III. Summary of the TLDs (TLD-100H model) experimental procedure.

Procedure	Actions
1. Reading	• Anneal and read the TLDs according to the chip manufacturer specifications. In the case of TLD-100H, the time-temperature profile requires a preheating phase (10 s at 135°C), acquisition phase (23 1/3 s at 240°C with a rate of 10°C/s) and annealing phase (10 s at 240°C) • Improve the accuracy by letting nitrogen gas flow through the dosimeter during the entire cycle
2. Sensitivity	• Expose all TLDs to the same radiation field • Evaluate the sensitivity factor as the ratio between the single-chip reading and the average-sample reading
3. Calibration	• Expose TLDs to different air kerma values • The TLDs response is linear in the mammography dose range • Evaluate each calibration point by averaging over three TLDs
3. Phantom Measurements	• Place the TLDs in the desired position within the phantom. TLDs have no orientation preference • Evaluate the dose value by averaging three exposures • Evaluate the combined standard uncertainty

2.E. Geant4 Monte Carlo simulation

Geant4 is a MC toolkit capable of simulating the physics processes of transportation and interaction of photons and electrons with matter.[40] A previously developed MC code[5,41] based on the Geant4 toolkit (release 10.03, December 2016) was modified to estimate the local dose within a breast phantom. The breast phantom used for the experimental measurements [shown in Fig. 2(a)] was implemented in the simulation as a voxelized volume. Although in this way a different material can be assigned to each voxel, in this work, all voxels are defined as representing the 50% glandular composition of the CIRS phantom, as specified by Byng et al.[42] It should be noted that the chemical composition and density described by Byng et al.[42] is slightly different from the one commonly used for breast applications[8] but it replicates, to the best of our knowledge, the phantom employed in this study. No difference was found if the phantom is modeled as a simple solid or as a voxel-based solid.[43]

All the physics processes, including photoelectric effect, Compton scattering, and Rayleigh interaction, were implemented in the MC code[44] using the EPDL97 library[45] using the Geant4 electromagnetic PhysicsList Option 4.[1] The default cut range for photons was used (1 mm, corresponding to an energy of 2.65 keV in 50% glandular breast tissue).

In order to replicate the dosimeter placement in Fig. 2(a), 30 sensitive volumes were implemented reproducing the TLD characteristics (i.e., dimensions and relative chemical composition of 99.5% LiF, 0.2% Mg, 0.004% Cu, and 0.296% P). The dose evaluated in each sensitive volume (D_{MC}) was tallied and then converted to air dose, according to the formula

$$D_{Air} = D_{MC} \frac{\left(\frac{\mu_{en}}{\rho}\right)_{Air}}{\left(\frac{\mu_{en}}{\rho}\right)_{TLD}} \quad (11)$$

where $\frac{\left(\frac{\mu_{en}}{\rho}\right)_{Air}}{\left(\frac{\mu_{en}}{\rho}\right)_{TLD}}$ is equal to 0.808 and represents the ratio of the mass energy-absorption coefficients at 20 keV for dry air and the TLD material, respectively, both evaluated according to the NIST database.[46]

[1]http://geant4.cern.ch/collaboration/working_groups/electromagnetic/physlist10.0.shtml

The irradiation beam in the simulation consisted of a rectangular, planar source of dimensions 12 cm × 20 cm emitting monoenergetic parallel x rays toward the phantom. For each simulation, 10^{10} photons were simulated to obtain a statistical uncertainty, estimated using the method proposed by Sempau et al.,[47] below 0.5% for all dose estimates. The simulation time (five parallel runs of 2×10^9 photons) was in the order of 24 h (on a 3.0 GHz Intel Xeon CPU E5-2690 v2 computer).

Scoring was performed over a 2D dose map by simulating, at the phantom depth being investigated, a layer of dimensions $12 \times 20 \times 0.038$ cm^3 of TLD material.

To normalize the photon fluence in the MC simulation to that used in the experiments, a scale factor was used, defined as the ratio between the experimentally used air kerma, measured by the IOC chambers (i.e., 13.8 mGy), and the simulated air kerma, analytically evaluated in the MC code (i.e., 0.014 mGy).

The formula used for the analytical evaluation of the air kerma is

$$K = \sum_i \frac{E_i \times \frac{\mu_{en}}{\rho}(E_i)}{S \times cos\theta_i} \tag{12}$$

where E_i is the energy of the i-th photon across a scoring surface of area S, $\frac{\mu_{en}}{\rho}(E_i)$ is the mass energy-absorption coefficient of the dry air at photon energy E_i obtained according to the NIST database[46] and θ_i is the angle between the photon direction and the direction perpendicular to S. Although the mass energy-transfer coefficient should be used[48] in Eq. (12) instead of the mass energy-absorption coefficient, for low-energy photons $\frac{\mu_{tr}}{\rho}$ is equal to $\frac{\mu_{en}}{\rho}$.

In the case of monochromatic parallel beam irradiation, K can be easily calculated as $\theta_i = 0°$ so $cos\theta_i = 1$. The accuracy of this approach was investigated by comparing the value obtained using Eq. (12) with the dose in air calculated in a sensitive volume of air ($5 \times 5 \times 1$ cm^3) irradiated by 10^9 monochromatic photons emitted by a 10×10 cm^2 isotropic planar rectangular source. In this situation of charged particle equilibrium, the dose in air is equivalent to the air kerma.[49]

In addition, to test the appropriateness of Eq. (12), a second simulation was performed with the beam at an incidence angle of 45°.

3. RESULTS

3.A. Dosimeter characterization

Figure 3 shows the calibration curves as a function of air kerma for the three fitting curves [Eq. (5)] for the XR-QA2 GafChromic™ films. The dashed blue lines refer to a fit computed when all the experimental values (i.e., up to 20 mGy) are considered, while solid red lines refer to a fit computed considering only values up to 10 mGy. All three fit functions show good chi-square values and no differences are found between dashed blue (i.e., all points) and solid red (i.e., only 7 points) lines.

Figure 4 shows the one-sigma uncertainty analysis for the calibration curves when only seven values are considered for the fit. The logarithmic function [Fig. 4(a)] gives a total uncertainty of less than 5% above 6 mGy air kerma, while the total uncertainty for the rational and exponential functions increases with increasing air kerma, due to the higher fit error on the parameters b and m, respectively. The best-fit function for the total uncertainty points (obtained using the software TableCurve 2D) is also reported in Fig. 4(a).

Figure 5 shows the sensitivity of the GafChromic™films and MOSFET detectors as a function of energy. Sensitivity constantly increases with photon energy for both dosimeters. In particular, it increases by ~48% for XR-QA2 films and by ~37% for MOSFET in the energy interval 18–28 keV.

The single calibration factors for MOSFET [i.e., CF_i in Eq. (7)] vary from a minimum value of (2.36 ± 0.09) mV/mGy to a maximum value of (2.43 ± 0.09) mV/mGy.

When using the TLDs, the dose is evaluated using Eq. (9): the calibration factor [i.e. K_{calib} in Eq. (9)] is $(2.21 \pm 0.03) \times 10^{-3}$ mGy/nC and the individual sensitivity factor [i.e., S_i in Eq. (9)] varies from a minimum value of (0.87 ± 0.03) to a maximum value of (1.10 ± 0.03).

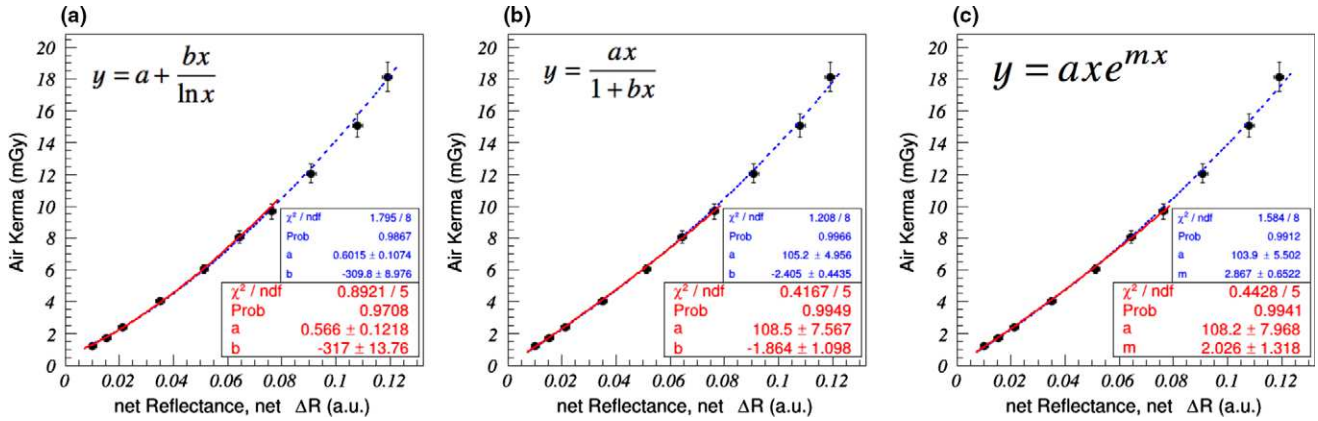

FIG. 3. Dose–response curves for the XR-QA2 GafChromic™ film evaluated using (a) logarithmic function, (b) rational function, and (c) exponential function. Dashed blue lines refer to a fit computed using all the values (i.e., up to 20 mGy), while solid red lines refer to a fit computed using only the values up to 10 mGy. [Color figure can be viewed at wileyonlinelibrary.com]

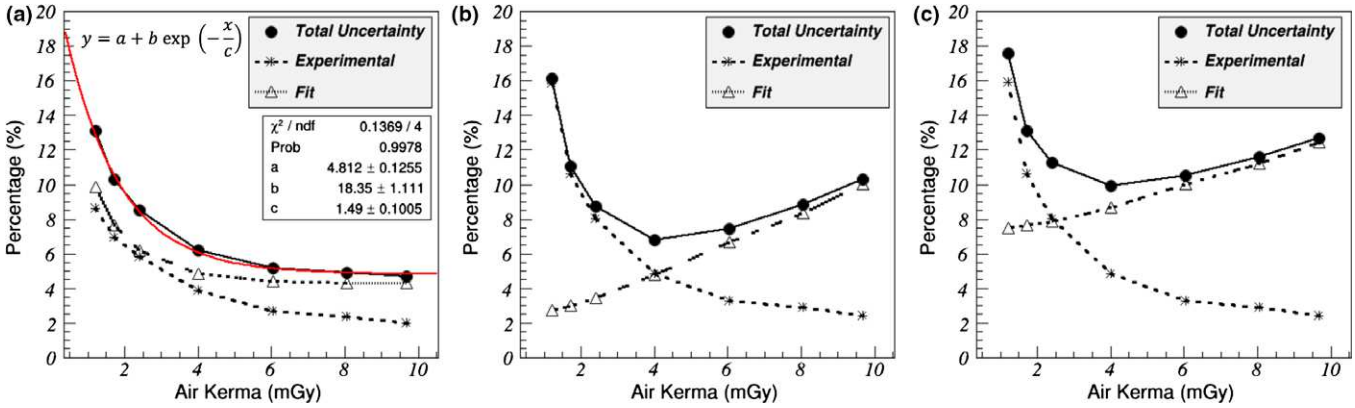

FIG. 4. One-sigma uncertainty analysis (total, experimental, and fitting) for the three calibration fitting functions: (a) logarithmic, (b) rational, and (c) exponential. In (a) the best-fit function for the total uncertainty is reported with a solid red line. [Color figure can be viewed at wileyonlinelibrary.com]

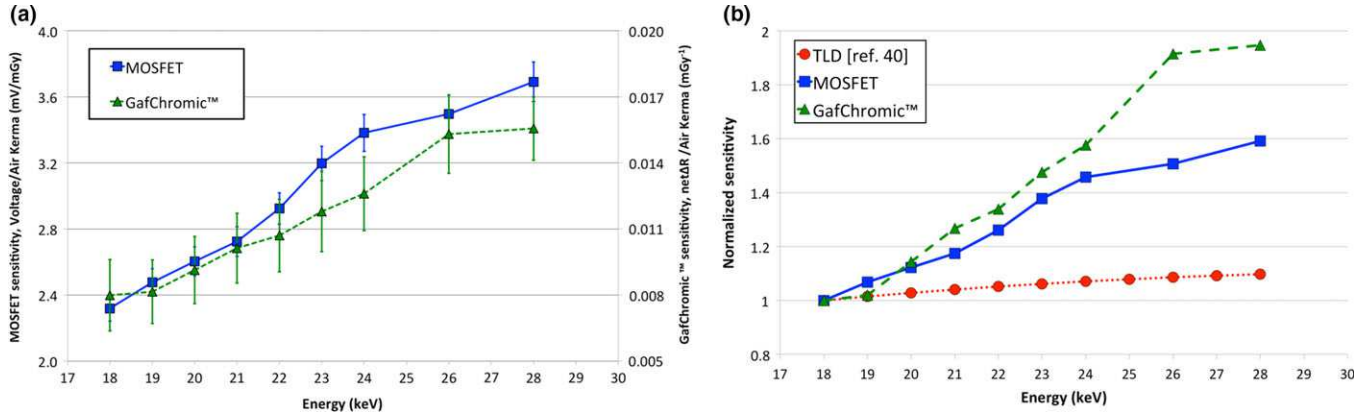

FIG. 5. (a) MOSFET (blue squares, on the left vertical axis) and GafChromic™(green triangles, on the right vertical axis) sensitivity as a function of monochromatic x-ray energy. The nominal air kerma was ~3.8 and ~3.5 mGy for MOSFET and GafChromic™, respectively. (b) TLD (red dots), MOSFET (blue squares) and GafChromic™(green triangles) sensitivity normalized to unity at the energy of 18 keV. Data for TLD are readapted from the work of Duggan et al.[39] [Color figure can be viewed at wileyonlinelibrary.com]

3.B. Monte Carlo validation and dose distribution analysis

Table IV reports the results for the air kerma investigation. As can be seen, the air kerma analytically evaluated using Eq. (12) is compatible, within the MC uncertainty of 1%, to the simulated calculated dose in air. Thus, the approach proposed for calculating the air kerma using Eq. (12) can be considered valid.

The comparison among all experimental measurements and TLDs-MC simulation for the depth of 1 cm is shown in Fig. 6. The results for all other phantom depths can be found in Figures S1, S2 and S3. A good agreement, within one combined standard uncertainty (k = 1), is found among all experimental data at all depths. When a higher coverage factor is used to extend the confidence interval up to 95% (i.e., k = 2) or 99.7% (i.e., k = 3) all measurements are comparable. As expected, a symmetric trend is noticeable when comparing values for the same location (e.g., #1 and #7, #2 and #6, #3 and #5, etc.).

The relative percentage difference [i.e., (TLD dose − MC dose)/MC dose] is lower than ± 5% (Fig. 7).

Table V reports the range in variation of the combined standard uncertainty (k = 1) for the three dosimeters. As can be seen, as the phantom depth increases, the percentage uncertainty also increases.

Figure 8 shows the mean dose value obtained when averaging all thirty dosimeters. Between the entrance and the 3 cm deep layer, the average dose decreases by ~80%.

Figures 9 and 10 show the 2D dose maps for GafChromic™ films and for the MC code, respectively. The two pieces of GafChromic™ film used to cover the entire phantom can be easily recognized in Fig. 9: the central horizontal line represents the line along which the two pieces were reassembled using the MATLAB code and explains the discontinuity in the results.

TABLE IV. Comparison of the analytical air kerma evaluation using Eq. (12) and the dose in air evaluated with the MC code for a monoenergetic photon beam at two different incidence angles.

Incidence angle	Air kerma	Dose in air
$\theta = 0°$	17.3 μGy	(17.4 ± 0.2) μGy
$\theta = 45°$	24.5 μGy	(24.5 ± 0.2) μGy

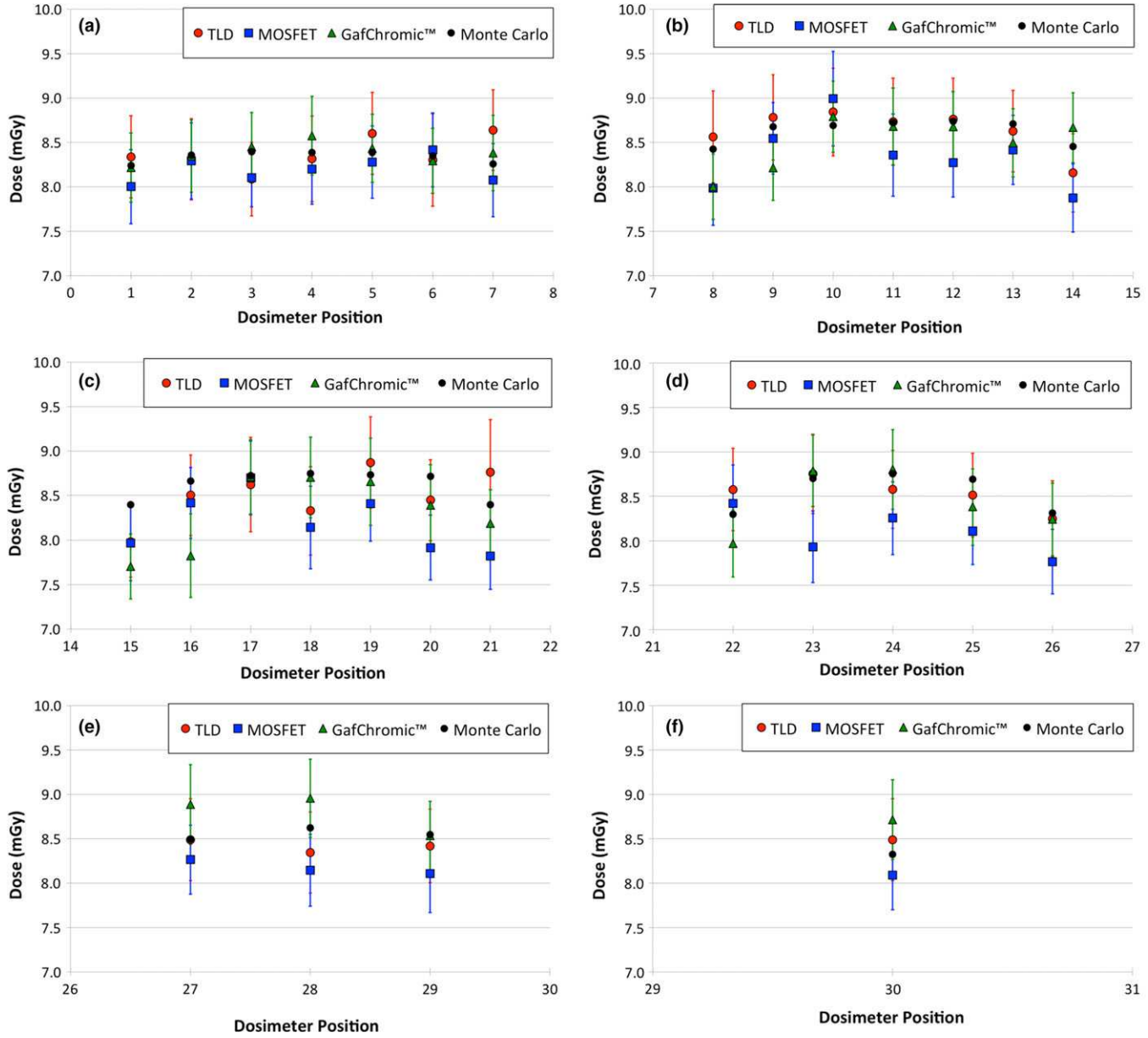

FIG. 6. Dose comparison between TLD (red dots), MOSFET (blue squares), GafChromic™ film (green triangles) and Monte Carlo simulations (black dots) for the 1-cm depth. In all graphs the uncertainty bars refer to the combined standard uncertainty (k = 1) and the dosimeter positions refer to Fig. 2(a). [Color figure can be viewed at wileyonlinelibrary.com]

A more homogeneous dose distribution is visible in the MC maps compared to the experimental ones.

However, once the uncertainty of the experimental measurements is taken into account (Figs. 11 and 12), it can be seen that the MC and experimental maps are compatible.

Profiles along the central chest-wall to nipple region [i.e., from dosimeter position #4 to #30 in Fig. 2(a)] and along the chest-wall side [i.e., from dosimeter position #1 to #7 in Fig. 2(a)] are shown in Figs. 11 and 12, respectively. The experimental values are all compatible with a flat behavior across the phantom, while the MC data show higher dose values at the phantom center and lower values at the border. The MC dose increment toward the phantom's center can be explained by the increase in contribution from scattered radiation.[50]

4. DISCUSSION

Dose estimation in mammography has been studied extensively over the last two decades. However, recent works based on dedicated breast computed tomography reported a dose overestimation when simple breast models are used.[5,6] To overcome the issues and limitations in current breast dosimetry methods, the American Association of Physicists in Medicine (AAPM) and the European Federation Of Medical Physics (EFOMP) have formed a joint Task Group to develop a new methodology to estimate breast dose.[7] The primary aim of this study was to review the methodology required for three different experimental internal breast dosimetry methods and to investigate their capabilities. Moreover, this study aimed to validate the dose estimation of MC simulations at

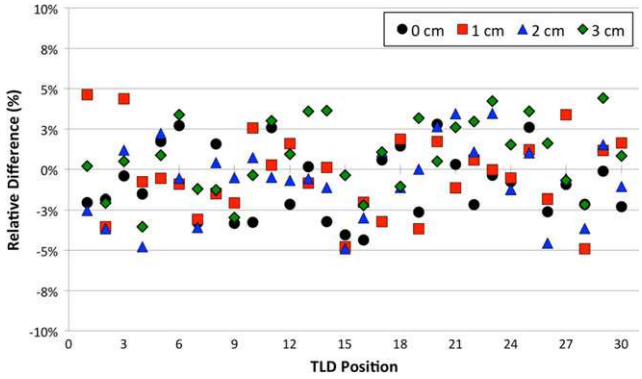

FIG. 7. Relative difference between the TLD and Monte Carlo data for the four investigated depths: black dots for 0 cm, red squares for 1 cm, blue triangles for 2 cm and green diamonds for 3 cm. The dosimeter positions are those shown in Fig. 2(a). [Color figure can be viewed at wileyonlinelibrary.com]

TABLE V. Range of the combined standard uncertainty (k = 1) for all three dosimeters (TLD, MOSFET, and GafChromic™) at the four depths.

	TLD (%)			MOSFET (%)			GafChromic™ (%)		
	Min	Mean	Max	Min	Mean	Max	Min	Mean	Max
Depth									
0 cm	5.0	5.6	6.4	4.6	4.9	5.5	4.1	4.7	7.1
1 cm	5.0	5.6	6.8	4.1	4.9	5.9	4.4	4.9	6.0
2 cm	5.0	5.7	7.1	4.6	5.3	6.8	4.5	5.6	7.9
3 cm	5.0	5.7	7.7	4.6	5.8	7.6	6.3	7.9	9.0

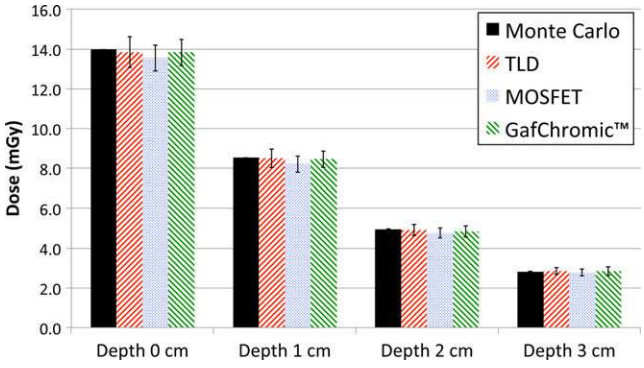

FIG. 8. Mean dose obtained by averaging all 30 values as a function of the increasing depth. The uncertainty bars refer to the combined standard uncertainty (k = 1). [Color figure can be viewed at wileyonlinelibrary.com]

the local level within and throughout the breast. This level of validation could be important for the estimation of breast dose in nonhomogeneous and/or nonuniform breast models. The idealized and simplified conditions provided by monochromatic SR were chosen as a first step, before moving to a clinical setting.

It was determined that XR-QA2 GafChromic™ films have a strong energy dependence with a maximum variation of about 48%, which is higher than the 30% previously found by Di Lillo et al.[21], albeit the two curves follow the same trend. This discrepancy can be due to the fact that in Di Lillo et al.[21] the sensitivity is evaluated at higher air kerma (i.e., 10 mGy instead of 3.5 mGy used in the present work), which lead to a higher reflectance change [i.e., netΔR, Eq.(1)]. All three functions reported in Eq. (5) fitted well the experimental data when all the values up to 20 mGy are used. However, if only the values up to 10 mGy are considered, better results in terms of fit precision and accuracy are obtained by the logarithmic functions, successfully used by other authors.[37,51]

The response of the MOSFET dosimeters increased with energy: a maximum variation of about 37% is found in the energy interval 18–28 keV. Thus, separate calibrations are also required for these dosimeters. However, the MOSFET calibration requires less time than XR-QA2 GafChromic™ due to their fast and simpler read-out process.

The TLD response was not investigated in this work due to the large amount of published literature on this topic.[12,16–18,39] Nevertheless, it is worthwhile to mention that TLDs also require separate calibration which lead to a significant postexposure processing (see Section 2.D).

Following the dosimeter preparation procedures described in Section 2, very good agreement is found between all experimental data and the MC results within the combined standard uncertainty (Fig. 6). A relative difference lower than 5% was found when MC results were compared to the TLD values (Fig. 7). This is a remarkable result considering the difficulties and inherent uncertainty in these types of measurements[1]: all the percentage combined standard uncertainty (k = 1) reported in Table V are below the recommended value of ± 12.5% set by the IAEA.[28] Thus, the MC code, within the limits of experimental uncertainty, can be considered validated. It should be noted that the uncertainty tends to increase with depth. This trend is more noticeable for GafChromic™ films and MOSFET than TLDs due to the fact that the former are less sensitive to dose and at certain depths are actually functioning close to the limits of detectability. Therefore, the percentage contribution of Type A uncertainties for GafChromic™films [i.e., u^2_{ROI} in Eq. (6)] and for MOSFET [i.e., $u^2_{\Delta V}$ and u^2_{CF} in Eq. (10)] increase approaching the low boundary of the detection range.

An experimental dose variation up to ~80% is observed with increasing depth (Fig. 8). This result is in agreement with the previous work of Sechopoulos et al.[52] where a variation between ~15% and ~400% is presented.

Experimental 2D dose maps obtained using XR-QA2 GafChromic™ films showed a nonhomogeneous dose pattern with visible longitudinal lines across the phantom. These findings are not confirmed with the MC simulations (Fig. 10). These differences are attributable to the GafChromic™ films, which required special attention prior to their use. First, to use the uniform response scanner area the film had to be cut in two parts and not exposed simultaneously: in this lapse of time (required to change the film) the current on the ELETTRA storage ring may vary slightly, causing a different irradiation condition. This effect, albeit small, can be significant. Second, the chemical composition of the GafChromic™ sensitive layer may vary not only between

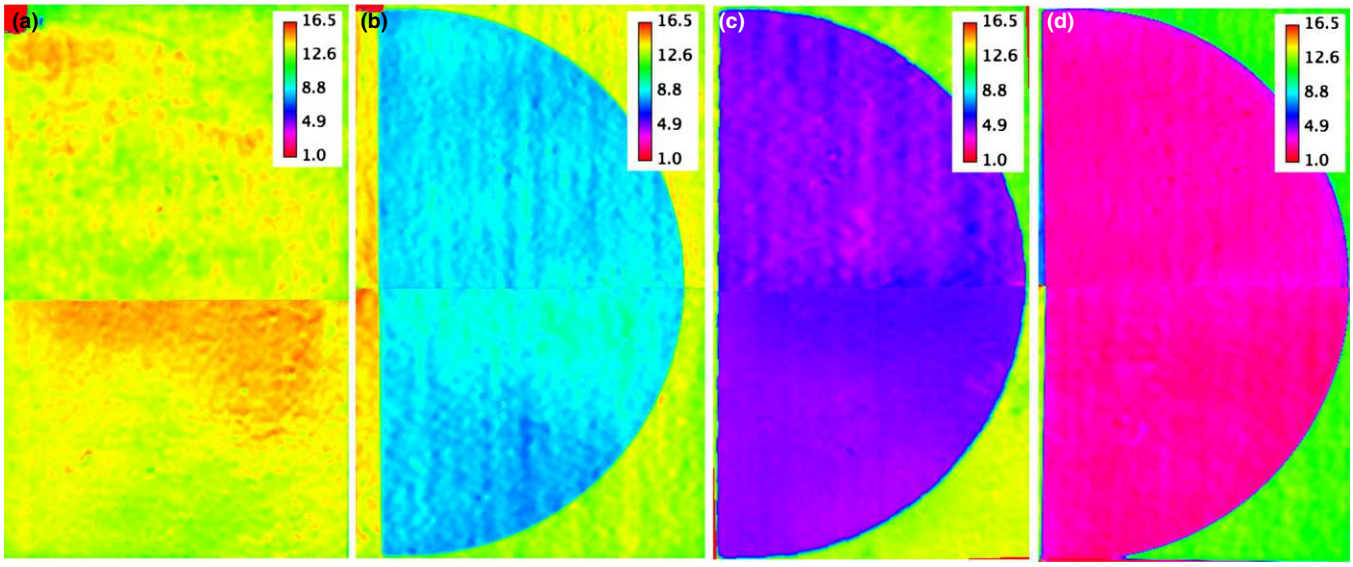

FIG. 9. 2D dose map obtained using the GafChromic™ film for the four investigated depths: (a) 0 cm, (b) 1 cm, (c) 2 cm, and (d) 3 cm. The values shown in the color legends are in units of mGy. [Color figure can be viewed at wileyonlinelibrary.com]

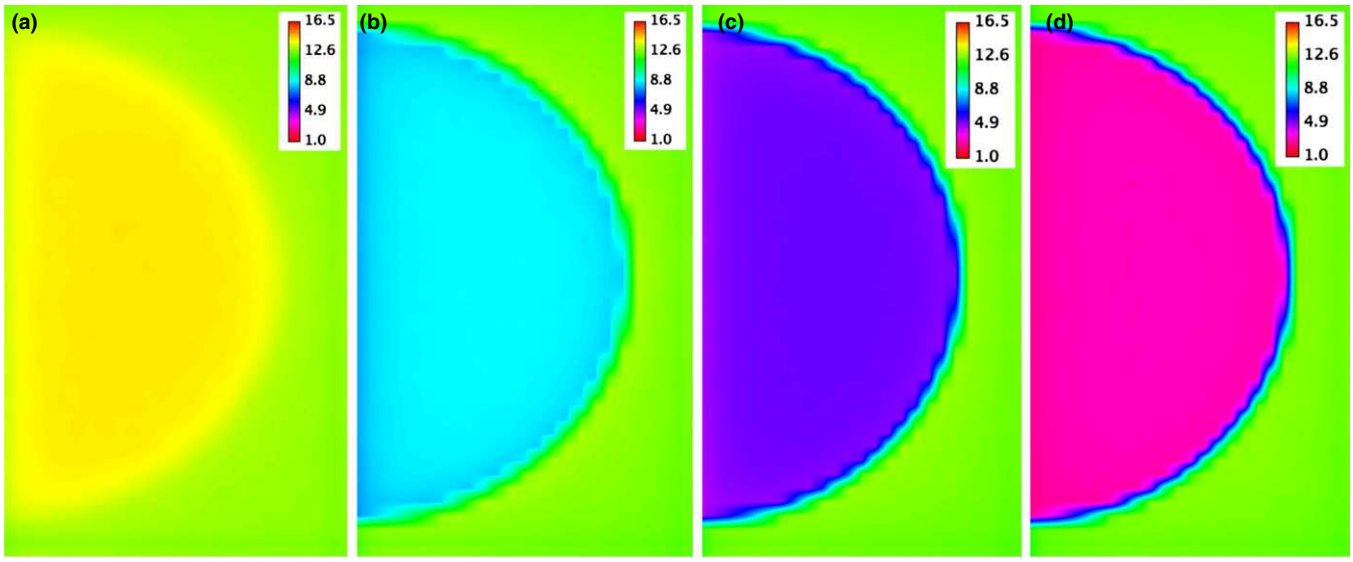

FIG. 10. Monte Carlo 2D dose map for the four investigated depths: (a) 0 cm, (b) 1 cm, (c) 2 cm, and (d) 3 cm. The values in the legend are in units of mGy. [Color figure can be viewed at wileyonlinelibrary.com]

different film batches but even within the same batch.[32,53] Moreover, the method used to spread out the sensitive layer is not uniform (according to the manufacturer specification, uniformity is < 7% before the irradiation). After the exposure, the inhomogeneity of the sensitive layer might be enhanced. These effects can explain the nonuniform dose distribution found for the GafChromic™ films reported in Fig. 9.

All the experimental profiles (reported in Figs. 11 and 12) are compatible with a uniform dose distribution while the MC shows higher dose values at the center of the phantom. This MC trend is qualitative comparable to that previously found by Sechopoulos et al.[50] who reported an increase in the scatter contribution toward the center of the phantom. This increment extends about 2 cm from the phantom edges in that work, comparable to the length of the effect described by the dotted-black profiles reported in Figs. 11 and 12.

The discrepancies at the phantom's edges between the experimental measurements and the MC output (Figs. 11 and 12) can be potentially explained considering the angular dependence of the dosimeters,[14,32] which is not modeled into the MC simulations.

It should be pointed out that, in order to detect a dose value at a depth of 3 cm, the delivered incident air kerma was 13.8 mGy. This value is higher than the clinical entrance skin dose of about 1.4 mGy for the same 3 cm phantom, obtained

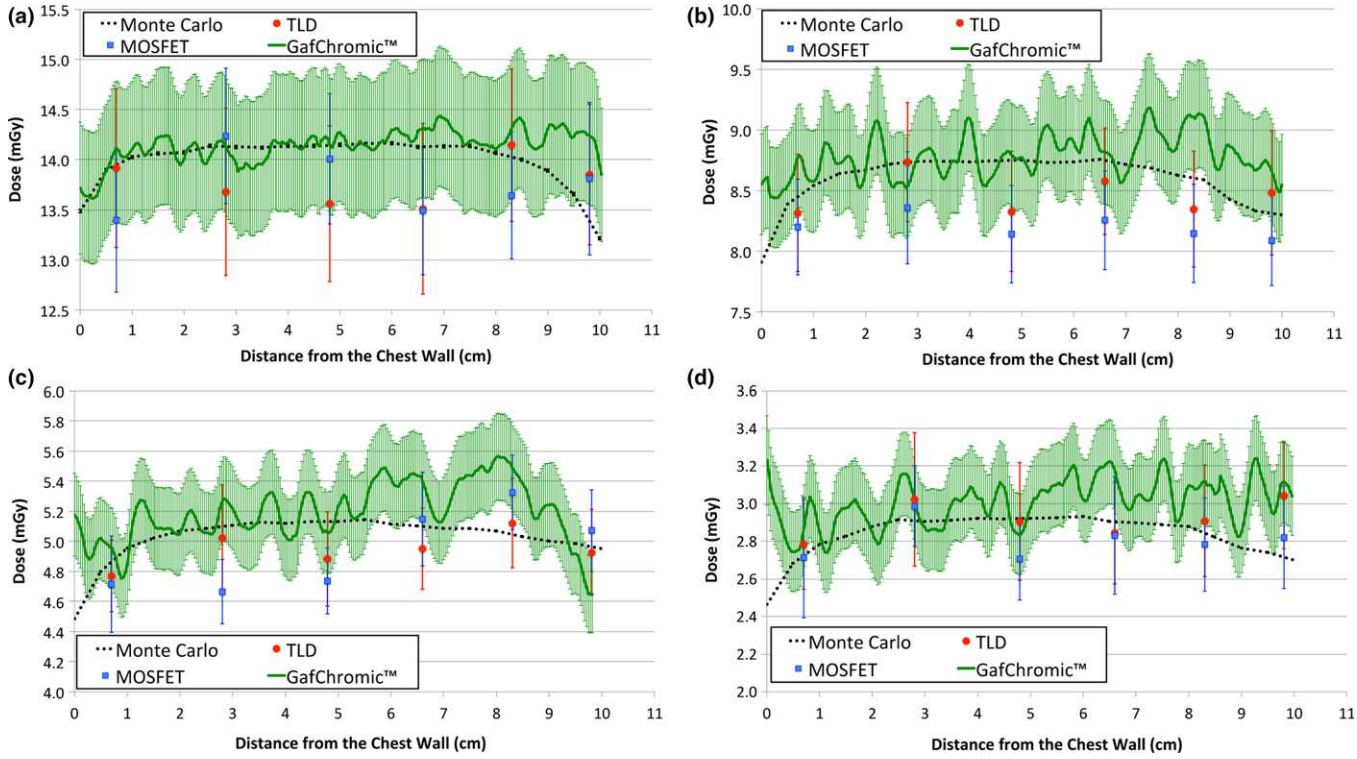

FIG. 11. Chest wall to nipple central profile comparing the experimental data obtained using TLD (red dots), MOSFET (blue squares), GafChromic™ film (green-solid line) and the Monte Carlo data (dotted-black line) for (a) 0 cm, (b) 1 cm, (c) 2 cm, and (d) 3 cm depths. The uncertainty bars represent the combined standard uncertainty (k = 1). [Color figure can be viewed at wileyonlinelibrary.com]

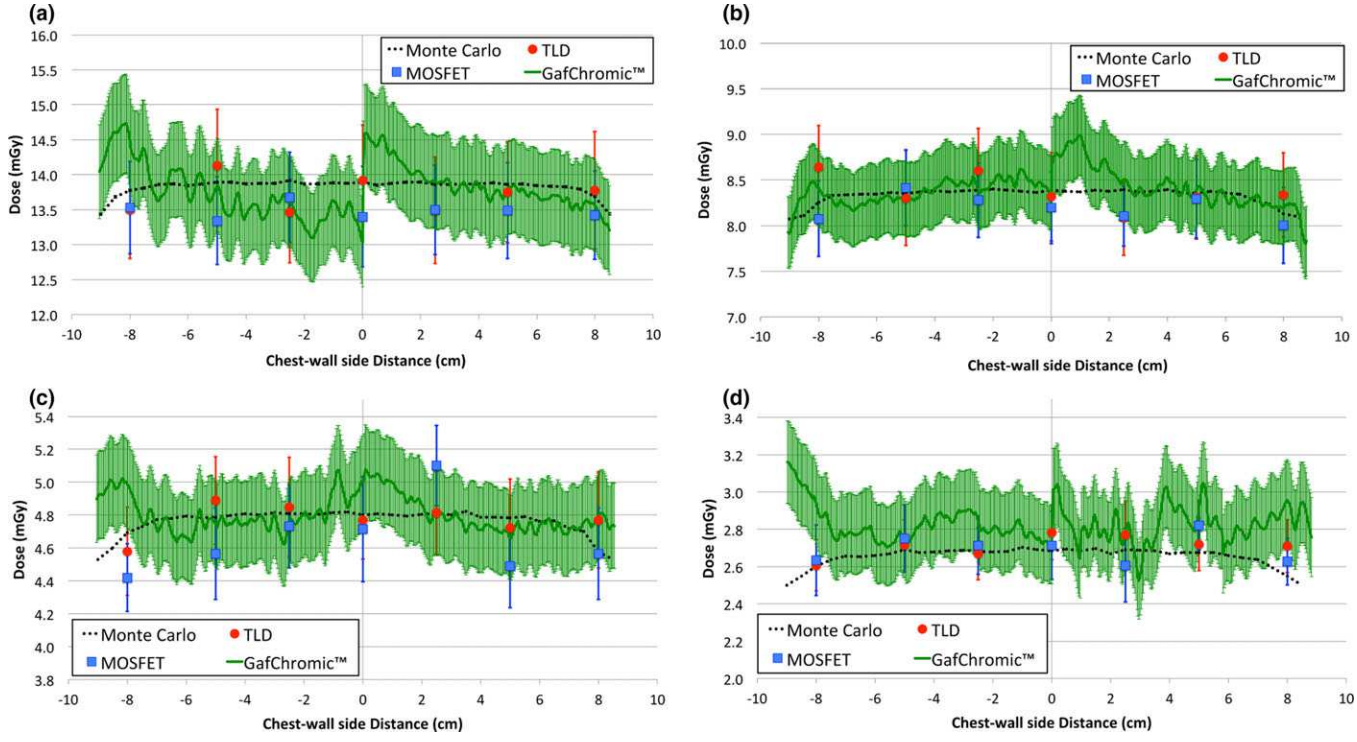

FIG. 12. Chest wall side profile which comparing the experimental data obtained using TLD (red dots), MOSFET (blue squares), GafChromic™ film (green-solid line), and the Monte Carlo data (dotted-black line) for (a) 0 cm, (b) 1 cm, (c) 2 cm, and (d) 3 cm depths. The uncertainty bars represent the combined standard uncertainty (k = 1). [Color figure can be viewed at wileyonlinelibrary.com]

using the automatic exposure control of a SIEMENS Mammomat Inspiration system with a W/Rh 28 kVp spectrum at 41.3 mAs. Thus, to achieve comparable measurements to those reported here, an air kerma similar to the one delivered at the synchrotron facility should be used. For example, for this phantom measurement with the SIEMENS system, a tube current-exposure time product of 360 mAs would need to be selected.

5. CONCLUSIONS

Proper experimental methodologies for internal breast dosimetry have to be used in order to estimate the dose with good accuracy. In this work, the performances of three dosimeters (GafChromic™ films, MOSFET and TLDs) were investigated and three corresponding experimental procedures were proposed.

It was found that the energy dependence of the tested dosimeters needs to be taken into account. In particular, for GafChromic™ our results lead to two important conclusions: (a) separate calibration curves should be obtained and applied at each photon energy or each beam quality, and (b) calibration curves, based on logarithmic functions, can be derived for a lower dose range (i.e., 1–10 mGy), reducing the effort required for this process.

The experimental procedures can be applied to validate Monte Carlo simulations for internal breast dose estimation: comparison of the Monte Carlo estimates showed agreement with the empirical measurements within the experimental uncertainty. This is a relevant result, which not only shows the appropriateness of the experimental procedures used but also of the simulation parameters.

ACKNOWLEDGMENTS

The authors thank the radiation protection staff of ELETTRA Sincrotrone Trieste (Italy) and in particular Dr. Giuliana Tromba and Dr. Katia Casarin for their help in the preparation of the measurements. Luca Brombal, PhD student of the University of Trieste, is also acknowledged for his support during the measurements. This work has been supported in part by NWO Exacte en Natuurwetenschappen (Physical Sciences) for the use of supercomputer facilities, with financial support from the Nederlandse Organisatie voor Wetenshappelijk Onderzoek (Netherlands Organization for Scientific Research, NWO), and by the Susan G Komen Foundation for the Cure (IIR13262248).

CONFLICTS OF INTEREST

The authors have no relevant conflicts of interest to disclose.

[a]Author to whom correspondence should be addressed. Electronic mail: ioannis.sechopoulos@radboudumc.nl

REFERENCES

1. Dance DR, Sechopoulos I. Dosimetry in x-ray-based breast imaging. *Phys Med Biol*. 2016;61:R271–R304.
2. Dance DR, Skinner CL, Young KC, Beckett JR, Kotre CJ. Additional factors for the estimation of mean glandular breast dose using the UK mammography dosimetry protocol. *Phys Med Biol*. 2000;45:3225–3240.
3. Wu X, Gingold EL, Barnes GT, Tucker MD. Normalized average glandular dose in molybdenum target-rhodium filter and rhodium target-rhodium filter mammography. *Radiology*. 1994;193:83–89.
4. Dance DR, Hunt RA, Bakic PR, et al. Breast dosimetry using high-resolution voxel phantoms. *Radiat Prot Dosim*. 2005;114:359–363.
5. Sechopoulos I, Bliznakova K, Qin X, Fei B, Feng SSJ. Characterization of the homogeneous tissue mixture approximation in breast imaging dosimetry. *Med Phys*. 2012;39:5050–5059.
6. Hernandez AM, Seibert JA, Boone JM. Breast dose in mammography is about 30% lower when realistic heterogeneous glandular distributions are considered. *Med Phys*. 2015;42:6337–6348.
7. American Association of Physicists in Medicine. Website: https://www.aapm.org/org/structure/?committee_code=TG282. Accessed January, 2018.
8. Sechopoulos I, Ali ESM, Badal A, et al. Monte Carlo reference data sets for imaging research: executive summary of the report of AAPM Research Committee Task Group 195. *Med Phys*. 2015;42:5679–5691.
9. Boone JM, Shah N, Nelson TR. A comprehensive analysis of DgNCT coefficients for pendant-geometry cone-beam computed tomography. *Med Phys*. 2004;31:226–235.
10. Mettivier G, Fedon C, Di Lillo F, et al. Glandular dose in breast computed tomography with synchrotron radiation. *Phys Med Biol*. 2016;61:569–587.
11. Warren-Forward HM, Duggan L. Towards in vivo TLD dosimetry in mammography. *Br J Radiol*. 2004;77:426–432.
12. Bastos FC, Castro WJ, Squair PL, Nogueira MS, Da Silva TA. Feasibility of calibrating thermoluminescent dosimeters in a mammography unit for patient dosimetry. *Radiat Meas*. 2011;46:2094–2096.
13. Dong SL, Chu TC, Lee JS, et al. Estimation of mean glandular dose from monitoring breast entrance skin air kerma using a high sensitivity metal oxide semiconductor field effect transistor (MOSFET) dosimeter system in mammography. *Appl Radiat Isot*. 2002;57:791–799.
14. Benevides LA, Hintenlang DE. Characterization of metal oxide semiconductor field effect transistor dosimeters for application in clinical mammography. *Med Phys*. 2006;33:514–520.
15. Soliman K, Bakkari M. Examination of the relevance of using radiochromic films in measuring entrance skin dose distribution in conventional digital mammography. *Radiat Prot Dosim*. 2015;165:373–375.
16. Kron T, Duggan L, Smith T, et al. Dose response of various radiation detectors to synchrotron radiation. *Phys Med Biol*. 1998;43:3235–3259.
17. Emiro F, Di Lillo F, Mettivier G, et al. Energy response of GR-200A thermoluminescence dosemeters to ^{60}Co and to monoenergetic synchrotron radiation in the energy range 28-40 keV. *Radiat Prot Dosimetry*. 2015;168:40–45.
18. Dong SL, Chu TC, Lan GY, Wu TH, Lin YC, Lee JS. Characterization of high-sensitive metal oxide semiconductor field effect transitor dosimeters system and LiF: Mg, Cu, P thermoluminescence dosimeters for use in diagnostic radiology. *Appl Radiat Isot*. 2002;57:883–891.
19. Wang B, Xu XG, Kim CH. Monte Carlo study of MOSFET dosemeter characteristics: dose dependence on photon energy, direction and dosemeter composition. *Radiat Prot Dosimetry*. 2005;113:40–46.
20. Tomic N, Quintero C, Whiting BR, et al. Characterization of the calibration curves and energy dependence Gafchromic™XR-QA2 model based radiochromic film dosimetry system. *Med Phys*. 2014;41:062105. (9 pp).
21. Di Lillo F, Mettivier G, Sarno A, et al. Energy dependent calibration of XR-QA2 radiochromic film with monochromatic and polychromatic x-ray beams. *Med Phys*. 2016;43:583–588.
22. Castelli E, Tonutti M, Arfelli F, et al. Mammography with synchrotron radiation: first clinical experience with phase-detection technique. *Radiology*. 2011;259:684–694.
23. Gil S, Fernández M, Prezado Y, Biete A, Bravin A, Sabés M. Synchrtron radiation in cancer treatments and diagnostics: an overview. *Clin Transl Oncol*. 2011;13:715–720.

24. Bräuer-Krisch E, Adam JF, Alagoz E, et al. Medical physics aspects of the synchrotron radiation therapies: microbeam radiation therapy (MRT) and synchrotron stereotactic radiotherapy (SSRT). *Phys Med*. 2015;31:568–583.
25. Nesterets YI, Gureyev TE, Mayo SC, et al. A feasibility study of X-ray phase-contrast mammography tomography at the imaging and medical beamline of the Australian synchrotron. *J Synchrotron Radiat*. 2015;22:1509–1523.
26. Longo R. "Current studies and future perspectives of synchrotron radiation imaging trials in human patients. *Nucl Instrum Methods A*. 2016;809:13–22.
27. Longo R, Arfelli F, Bellazzini R, et al. Towards breast tomography with synchrotron radiation at Elettra: first images. *Phys Med Biol*. 2016;61:1634–1649.
28. International Atomic Energy Agency (IAEA). Dosimetry in diagnostic radiology: an international code of practice. Technical reports series No. 457 IAEA Vienna; 2007.
29. Joint Committee for Guides in Metrology. Evaluation of measurements data – Guide to the expression of uncertainty in measurement. *JCGM*; 2008.
30. Abrami A, Arfelli A, Barroso RC, et al. Medical application of synchrotron radiation at the SYRMEP beamline of ELETTRA. *Nucl Instrum Methods A*. 2005;548:221–227.
31. Bovi M, Laitano RF, Pimpinella M, et al. Absolute air-kerma measurement in a synchrotron light beam by ionization free-air chamber. Presented at the Worshop on Absorbed Dose and Air Kerma Primary Standards, Paris, 9-11 May 2007.
32. Giaddui T, Cui Y, Galvin J, Chen W, Yu Y, Xiao Y. Characteristics of GafChromic XRQA2 films for kV image dose measurements. *Med Phys*. 2012;39:842–850.
33. Butson E, Alnawaf H, Yu PKN, Butson M. Scanner uniformity improvements for radiochromic film analysis with matt reflectance backing. *Austr Eng Phys Sci Med*. 2011;34:401–407.
34. Alnawaf H, Yu P, Butson M. Comparison of Epson scanner quality for radiochromic film evaluation. *J Appl Clin Med Phys*. 2012;13:314–321.
35. Farah J, Trianni A, Ciraj-Bjelac O, et al. Characterization of XR-RV3 GafChromic™ films in standard laboratory and in clinical conditions and means to evaluate uncertainties and reduce errors. *Med Phys*. 2015;42:4211–4226.
36. Rampado O, Garelli E, Deagostini S, Ropolo R. Dose and energy dependence of response of Gafchromic® XR-QA film for kilovoltage x-ray beams. *Phys Med Biol*. 2006;51:2871–2881.
37. Tomic N, Devic S, Deblois F, Seutjens J. Reference radiochromic film dosimetry in kilovoltage photon beams during CBCT image acquaisition. *Med Phys*. 2010;37:1083–1092.
38. Devic S, Seuntjens J, Hegyi G, et al. Dosimetric properties of improved GafChromic films for seven different digitizers. *Med Phys*. 2004;31:2392–2401.
39. Duggan L, Hoodm C, Warren-Forward H, Haque M, Kron T. Variations in dose response with x-ray energy of LiF:Mg, Cu, P thermoluminescence dosimeters: implications for clinical dosimetry. *Phys Med Biol*. 2004;49:3831–3845.
40. Agostinelli S, Allison J, Amako K, et al. Geant4 – a simulation toolkit. *Nucl Instrum Methods A*. 2003;506:250–303.
41. Sechopoulos I, Suryanarayanan S, Vedantham S, D'Orsi C, Karellas A. Computation of the glandular radiation dose in digital tomosynthesis of the breast. *Med Phys*. 2007;34:221–232.
42. Byng JW, Mainprize JG, Yaffe MJ. X-ray characterization of breast phantom materials. *Phys Med Biol*. 1998;43:1367–1377.
43. Sarno A, Dance DR, van Engen RE, et al. A Monte Carlo model for mean glandular dose evaluation in spot compression mammography. *Med Phys*. 2017;44:3848–3860.
44. Fedon C, Longo F, Mettivier G, Longo R. GEANT4 for breast dosimetry: parameters optimization study. *Phys Med Biol*. 2015;60:N311–N323.
45. Cullen D, Hubbell JH, Kissel L. EPDL97: the Evaluated Photon Data Library, '97 version. UCRL-50400;6(5).
46. Hubbell JH, Seltzer SM. Tables of X-Ray Mass Attenuation Coefficients and Mass Energy-Absorption Coefficients from 1 keV to 20 MeV for Elements Z=1 to 92 and 48 Additional Substances of Dosimetric Interest. National Institute of Standard Technology (NIST). Web Site: https://www.nist.gov/pml/x-ray-mass-attenuation-coefficients.
47. Sempau J, Sánchez-Reyes A, Salvat F, Tahar HOB, Jiang SB, Fernández-Varea JM. Monte Carlo simulation of electron beams from an accelerator head using PENELOPE. *Phys Med Biol*. 2001;46:1163–1186.
48. International Commission on Radiation Units and Measurements (ICRU). *Fundamental Quantities and Units for Ionizing Radiation*. Report 85(11). Oxford: Oxford University Press; 2011.
49. Attix FH. *Introduction to Radiological Physics and Radiation Dosimetry*. New York, NY: Wiley; 1986.
50. Sechopoulos I, Suryanarayanan S, Vedantham S, D'Orsi CJ, Karellas A. Scatter radiation in digital tomosynthesis of the breast. *Med Phys*. 2007;34:564–576.
51. Di Lillo F, Dreossi D, Emiro F, et al. Use of XR-QA2 radiochromic films for quantitative imaging of a synchrotron radiation beam. *J Instrum*. 2015;10:C05002.
52. Sechopoulos I, Feng SSJ, D'Orsi CJ. Dosimetric characterization of a dedicated breast computed tomography clinical prototype. *Med Phys*. 2010;37:4110–4120.
53. Giaddui T, Cui Y, Galvin J, Yu Y, Xiao Y. Comparative dose evaluations between XVI and OBI cone beam CT system using GafChromic XRQA2 film and nanoDot optical stimulated luminescence dosimeters. *Med Phys*. 2013;40:062102. (12 pp.).

SUPPORTING INFORMATION

Additional Supporting Information may be found online in the supporting information tab for this article.

Fig. S1. Experimental dose comparison between TLD (red dots), MOSFET (blue squares), GafChromic™ film (green triangles), and Monte Carlo simulations (black dots) for the 0-cm depth. In all graphs the uncertainty bars refer to the combined standard uncertainty (k = 1) and the dosimeter positions refer to Fig. 2(a).

Fig. S2. Experimental dose comparison between TLD (red dots), MOSFET (blue squares), and GafChromic™ film (green triangles) and Monte Carlo simulations (black dots) for the 2-cm depth. In all graphs the uncertainty bars refer to the combined standard uncertainty (k = 1) and the dosimeter positions refer to Fig. 2(a).

Fig. S3. Experimental dose comparison between TLD (red dots), MOSFET (blue squares) and GafChromic™ film (green triangles) and Monte Carlo simulations (black dots) for the 3-cm depth. In all graphs the uncertainty bars refer to the combined standard uncertainty (k = 1) and the dosimeter positions refer to Fig. 2(a).